A Micro Model for Elasto-Plastic Adhesive-Contact in Micro-Switches: Application to cyclic loading

L. Wu[a,b,*], J.-C. Golinval[a], L. Noels[a]

[a] *University of Liège Aerospace and Mechanical Engineering Department*
Chemin des chevreuils 1, B-4000 Liège, Belgium
[b] *Northwestern Polytechnical University*
School of Aeronautics, 710072 Xi´ an, China

Abstract

Stiction is a major failure mode in micro-electromechanical systems. In previous works, a statistical rough surfaces interaction model, for which only elastic adhesive contact has been considered, was developed for multiscale analyzes.

However, during the impact between rough surfaces, plastic deformations of asperities cannot always be neglected. In the present work, the adhesion between rough surfaces is studied considering the elasto-plastic deformations of the asperities, and a model predicting the resulting micro adhesive-contact forces is derived.

For illustration purpose, an electrostatic-structural analysis is performed on a micro-switch. To determine the degree of plasticity involved, the impact energy of the movable electrode at pull-in is estimated. Thus the maximal adhesive force evolution during cyclic loading is predicted using the developed model.

Keywords: Stiction, Adhesion, Elasto-plasticity, Cyclic loading

1. Introduction

Micro-electromechanical systems (MEMS) in general, and micro-switches in particular, are becoming more and more popular due to their inherent advantages as their low production costs, their small sizes ... However, the resistance to stiction of micro-switches remains a major issue [1]. One of the most important failure mechanism of MEMS is stiction [2], which results from surface forces (capillary, van der Waals (VDW) or electrostatic). Indeed due to the reduced sizes of MEMS, surface forces become of the same order of magnitude as mechanical forces, and two components entering into contact could permanently adhere to each-other. This can happen either during the fabrication process at etching or during normal use, in which cases one will respectively talk about

*Corresponding author, Phone: +32 4 366 94 53, Fax: +32 4 366 95 05
Email address: L.Wu@ulg.ac.be (L. Wu)

release or in-use stiction. The risk of in-use stiction increases when plasticity is involved during the contact phase, as the contact surface of asperities increases. A comprehensive review of the experiments conducted and models developed to reduce the adhesion risk can be found in [3].

In order to improve the MEMS reliability to stiction, analytical models were first developed in the elastic range, in which case, when studying effects of van der Waals forces, they are commonly based on two theories of adhesion between two elastic spheres, the Johnson-Kendall-Roberts (JKR) model [4] and the Derjaguin-Muller-Toporov (DMT) model [5]. As the JKR model is ideal for compliant materials with a large contact curvature surface and with a high surface energy, while the DMT theory is well suited for stiff materials with a reduced contact curvature and with a low surface energy, Maugis [6] provided a transition solution for intermediate cases. In this model, the transition between the two regimes is characterized by the Maugis transition parameter λ, which involves surface and material properties. This model was improved to account for the adhesion in the non-contacting parts of the spheres by Kim *et al.* [7]. In order to account for the roughness property of real micro-surfaces, these former analytical theories based on a single asperity model can be generalized using the statistical approach introduced by Greenwood and Williamson (GW) [8], where the rough surfaces are simulated by multi-asperities with a random height distribution [9]. Such an approach was conducted by the authors in [10] in order to predict the micro adhesive-contact curves, *i.e.* the adhesive-contact force *vs.* the surface separation distance, for two interacting micro-surfaces.

To apply this micro-mechanical model, which has the advantage of accounting for a wide variety of micro-scale parameters (surface topography, surface cleanness, material parameters, environment...), two-scale approaches have recently been proposed in [11, 12]. In these works, a finite-element model of a MEMS device is studied, and when contact occurs between components, the micro adhesive-contact curves evaluated in [10], for the proper surface and material parameters, are used as a governing contact law. The authors have studied in [12] the stiction of micro-cantilever beams made of poly-silicon and have been able to predict, with a good accuracy, the cantilever critical length leading to permanent adhesion in a dry environment and for different surface roughness states. In particular the apparent adhesion energy predicted by this approach was in good agreement with literature data [13, 14].

Although promising for a design purpose, this methodology requires an accurate micro-model, and in particular, an accurate evaluation of the adhesive-contact force *vs.* the surface separation distance curves. To improve the accuracy, the extension of the micro-model to the elasto-plastic behavior, which can be present at the asperity level, is required for metallic contacts. This extension is the main aim of the present work.

During interactions of elasto-plastic rough surfaces, due to the statistical nature of the asperity distribution on the interacting surfaces, each asperity will be affected differently. Due to the plastic deformations of the higher asperities during contact, the contact force on the elasto-plastic deformed asperities is lower than in the elastic case for the same contact interference, while adhesive effects

increase due to the change of asperity profiles. As a consequence, the pull-out force defined as the maximum attractive forces or the minimum compressive forces between the two surfaces in contact is higher than that between two pure elastic contacting rough surfaces. After repeating contacts, the distribution of asperities height changes [15], as well as the tip radii of the higher asperities, until plastic accommodation, also called shakedown [16], is reached. This process was assimilated to contact hardening for micro-switches by Majumder *et al.* [17], as the pull-out force indeed increases until accommodation.

In order to develop a micro-model able to predict stiction for elasto-plastic rough surfaces, three steps are achieved in this paper: development of a model of a single elasto-plastic asperity - rigid flat plane interaction, generalization to the interaction of rough surfaces, and application of the model accounting for dynamic effects and cyclic loadings. Although general, the model requires finite-element results and is parametrized in this paper for Ruthenium surfaces only.

First, as what has been done in [10] in the elastic case, the single asperity/plane interaction problem is studied before extension to the interaction of two rough surfaces. During contacts, as a critical yield stress is reached, part of the material within the asperity yields gradually and some material is deformed plastically, while the surrounding material can remain elastic (elasto-plastic interim regime) or not (fully plastic regime). The truncation model was first developed by Abbott and Firestone (FA) [18] and Greenwood and Tripp [9] derived later a similar model, see the discussion of Jackson and Green [19] for more details. This model states that under fully plastic conditions the area of contact of an asperity pressed against a rigid flat surface can be approximately calculated by truncating the asperity tip. The Chang-Etsion-Bogy (CEB) model of a single sphere pressed by rigid flat plane [20] considers a constant volume when plasticity occurs, which cannot represent the interim elastic-regime in a single asperity. In their model, Sahoo and Banerjee [21] assumed that the asperity keeps the Hertz contact profile even under plastic behaviors, allowing the adhesive forces to be evaluated from the DMT adhesion model. Maugis-Dugdale theory [6] was used in Peng and Guo´ s work [22] to consider the adhesive interaction in the fully plastic regime. In these last two cases, the interim elasticplastic regime cannot be modeled either.

Apart from these analytical models for plasticity, models can also be based on numerical results. Based on finite element analysis results and considering the variation in the curvature of the contact surface during the contact interaction, an analogous theoretical model was deduced by Li *et al.* [23]. Kogut and Etsion (KE) [24, 25] developed a model based on finite-element results for an elastic-perfectly plastic sphere-plane interaction. In this model, a very detailed analysis of the stress distribution in the contact region is performed and the empirical expressions are presented for the contact area and for the contact force in a piece-wise form. In the work of Jackson and Green (JG) [19], a finite element analysis is also performed and the produced results appreciably differ from the KE model as the contact pressure in the fully plastic range was found to be a varying function of the yield strength and of the deformed geometry instead

of the sole hardness. The effect of contact condition (slip/stick) was described by Brizmer *et al.* [26]. In complement to these loading studies, the unloading behavior was also studied by Etsion *et al.* [27].

In these previous analyzes, the adhesive effect is not included to evaluate the asperity deformation. However this effect can become important for compliant elasto-plastic materials. Mohamed Ali and Sahoo [28] applied the JKR model [4] to consider the adhesive behavior of elasto-plastic and fully plastic regimes of contacting asperities. During the elasto-plastic regime, KE finite-element results were used in [28] to calculate the contact force and the interference was modified to account for the adhesion. In the fully plastic regime, the contact force was subtracted to represent the adhesive effect. Similarly, the adhesion due to the meniscus effect was introduced by Xue and Polycarpou [29] using the KE results. As Maugis theory [6] is an analytical theory based on the Dugdale assumption of inter-atomic attractions – within a critical distance, two surfaces are attracted with a constant force per unit area and if the separation exceeds this threshold, the adhesive traction immediately falls to zero – the model is unable to predict pre-contact deformations [30] resulting from the adhesive effect. The use of a Lennard-Jones (LJ) potential [31], substituting the Dugdale assumption for the adhesive part, shows hysteretic curves during transitions from no contact to contact conditions (jump-into-contact) and from contact to no contact conditions (jump-out of- contact) [32, 33]. In particular, a jump-in-induced yield criterion was developed in [32] based on semi-analytical results, and was exploited in [33] for cyclic loadings.

The generalization to two rough surfaces can be conducted by finite element simulations where the surfaces are discretized, as it has been proposed for elasto-plastic asperities by Pei *et al.* [34] without accounting for adhesion, or by Ardito *et al.* [35] with capillary and VDW effects. The treatment of rough surfaces can also be obtained from the single asperity study, by extending the GW-elastic formulation and by using the CEB single asperity model, [20]. The JG single asperity model [19] was combined to the statistical GW surface representation by Jackson and Green [36], while defining the limit of of the model in terms of contact area - asperity radius ratio. Another statistical model for the unloading of elasto-plastic rough surfaces based on the single asperity model [27] was presented by Kadin *et al.* [37]. Jackson and Streator [38] considered a multi-scale representation of the surfaces, alleviating the effect of sample size when defining surface representations from measured data. Beside being used for stiction studies, this model was used by Almeida *et. al* [39] to predict the effective contact resistance of a MEMS relay. A comparison of the different surface representation techniques for elasto-plastic problems was provided by Jackson and Green [40]. However these last generalizations do not account for adhesion. The adhesive effect was considered by Mukherjee and Sahoo [41] who combined the GW surface representation with the KE single asperity model [24, 25]. As an alternative to a GW surface representation, a fractal analysis of the surface was proposed by Komvopoulos and Yan [42] who accounted for plasticity and adhesive effects.

In this work, with the aim of predicting the stiction risk in switches, we

propose a model to predict the loading/unloading micro adhesive-contact curves of two interacting elasto-plastic rough surfaces. With a view to the use of this model in a future 2-scale MEMS study as in [12], this model should be fast to use, and highly parametrized.

In Section 2, following previous models, the elasto-plastic deformation resulting from the single asperity contact problem is first evaluated without considering the adhesive effect. Thus, although it enables the modelization of hysteretic curves between loading and unloading, adhesion-induced plasticity which could happen for extremely compliant materials as gold, see the criterion developed in [32, 33], will not be modeled. Using previous descriptions [19, 20, 23, 26, 27], the evaluation of the asperity profile during loading and unloading is obtained. As we neglect plastic deformations from the adhesive effect, we can consider the Maugis theory [6] completed by Kim extension [7] to evaluate the adhesive forces. This adhesion depends on the tip radius evolution during the loading process. As a main difference with previous models, adhesive forces are evaluated taking into account the effect of the non-constant asperity curvature after elasto-plastic deformations, which conducts to an accurate prediction of the pull-out forces when compared to full finite-elements simulations [31]. Only van der Waals forces are considered, which is a realistic assumption below 30 % humidity [2].

The interaction of two rough surfaces is achieved in Section 3 by considering a usual statistical distribution of asperities. The distribution of asperities height and the asperity profiles of the higher asperities change due to the plastic deformations. These changes are evaluated using the single asperity model, which also predicts the adhesive-contact forces. An integration on the surface leads directly to the sought micro adhesive-contact curves for loading and unloading of two interacting elasto-plastic rough surfaces.

Finally as an illustration purpose, a 1D micro-switch is studied in Section 4. Toward this end, the kinetic energy involved during the impact is evaluated from the pull-in analysis and is used to compute the elasto-plastic deformations. The adhesive-contact forces can be predicted during cyclic loading/unloading. It is shown that the repeated loading of a MEMS switch changes the structure of the contacting surfaces due to the plastic deformations, and as with time the contact surfaces become smoother, the adhesive effect increases until accommodation.

2. Single Asperity Model

In this section we study the micro adhesive-contact interaction between a single elasto-plastic asperity and a flat rigid surface. As a first step, the elasto-plastic deformation resulting from the single asperity contact problem is evaluated without considering the adhesive effect. As a result the model is not suited for extremely compliant materials for which adhesive forces before the contact onset could induce plasticity. As a second step, the adhesive effect due to the van der Waals forces is evaluated using Maugis theory [6] completed by Kim extension [7]. Toward this end, we propose to use an effective radius accounting

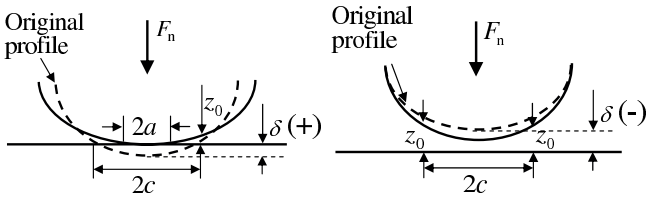

(a) Positive interference (b) Negative interference

Figure 1: Definition of the interference δ. (a) For a positive interference, a is the contact radius and c is the adhesive-contact radius. (b) For a negative interference, c is the adhesive-contact radius.

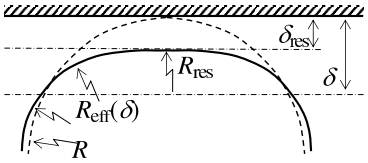

Figure 2: Evaluation of the effective radius R_{eff}

for the non-constant nature of the asperity curvature. Results are thus compared with FE simulations for the Ruthenium material. A brief description on how to identify the required parameters is also provided.

2.1. Elasto-Plastic Contact

When it comes to the study of a single asperity of tip radius R interacting with a plane, the interference δ is defined as the distance between the original profile of the asperity tip and the plane. It is positive in case of contact, and negative before the onset of contact, see Fig. 1. Following previous works [19, 20, 26], the critical yield interference δ_{CP} is defined as the interference at which the asperity starts yielding. The analogous numerical approximations of Chang *et al.* [20] and Jackson *et al.* [19] derive the critical interference from the von Mises yield criterion. The von Mises yield criterion is also applied by Brizmer *et al.* [26] to derive the critical interference analytically. All of them obtain the following form

$$\delta_{\text{CP}} = \left(\frac{\pi C_\nu S_Y}{2E} \right)^2 R \,, \tag{1}$$

where E is the asperity Young modulus, S_Y its yield stress, and where C_ν is a coefficient related to its Poisson coefficient ν. Chang *et al.* [20], Jackson *et al.* [19] and Brizmer *et al.* [26] propose three expressions producing almost indistinguishably results in the Poisson ratio validity range. In this paper, the form of Jackson *et al.* [19] $C_\nu = 1.295e^{0.736\nu}$ is adopted. The corresponding critical contact radius a_{CP} and contact force F_{CP} are respectively given by $a_{\text{CP}} = \sqrt{\delta_{\text{CP}} R}$ and $F_{\text{CP}} = \frac{2}{3}\pi C_\nu S_Y \delta_{\text{CP}} R$.

If during the loading phase, the interference goes beyond the critical interference δ_{CP} until reaching the maximal value $\delta_{\max}$, due to the plastic deformations

the effective asperity tip radius after unloading is different from its initial value R. The FE-based curve fitting achieved by Etsion *et al.* [27] leads to

$$\delta_{\text{res}} = \delta_{\max}\left[1-\left(\frac{\delta_{\text{CP}}}{\delta_{\max}}\right)^{0.28}\right]\left[1-\left(\frac{\delta_{\text{CP}}}{\delta_{\max}}\right)^{0.69}\right], \quad (2)$$

$$R_{\text{res}} = R\left[1+1.275\left(\frac{S_Y}{E}\right)^{0.216}\left(\frac{\delta_{\max}}{\delta_{\text{CP}}}-1\right)\right], \quad (3)$$

for respectively the residual interference δ_{res} and the residual curvature R_{res} of the sphere after complete unloading, see Fig. 2. This curve fitting holds for isotropic materials while $1 < \frac{\delta_{\max}}{\delta_{\text{CP}}} < 150$.

2.2. Adhesive-Contact

First we briefly review the Maugis [6] adhesive-contact theory combining Kim extension [7]. This adhesive-contact model for a single elastic asperity interaction includes the Hertz contact forces due to the elastic deformation of the asperity at micro contacts and the adhesive forces due to van der Waals attractive forces. A complete overview can be found in [10]. Then we propose an enhanced model to predict the loading and unloading adhesive-contact forces for a single elasto-plastic asperity.

2.2.1. Maugis Theory

In Maugis model, the inter-atomic attraction effect is modeled using the Dugdale assumption of inter-atomic attractions: within a critical value of separation z_0, two surfaces are attracted with a constant force per unit area σ_0, and if the separation z exceeds this threshold z_0, the adhesive traction immediately falls to zero. From this assumption the adhesive energy $\varpi = \sigma_0 z_0$ can be evaluated from the surface energies γ_i of the two interacting materials, with $\varpi = \gamma_1 + \gamma_2 - \gamma_{12}$, where γ_{12} is the interface energy.

In order to characterize the importance of the adhesive traction to the Hertz elastic deformation pressure, the Maugis transition parameter between the JKR and DMT regimes is defined as

$$\lambda = \frac{2\sigma_0}{\sqrt[3]{\frac{\pi\varpi K^2}{R}}}, \quad (4)$$

where $K = \frac{4}{3}\left(\frac{1-\nu_1^2}{E_1}+\frac{1-\nu_2^2}{E_2}\right)^{-1}$ depends on the material properties of the two bodies. In Eqn. (4), R is the initial tip radius of an asperity interacting with a plane, but the expression remains valid for the interaction of two spheres if $R = \frac{R_1 R_2}{R_1+R_2}$ is defined as the equivalent radius. The adhesive-contact force of the asperity F_{n} and the contact radius a can be obtained from the interference

δ, see Fig. 1(a) for schematics, by solving the system

$$\begin{aligned} 1 &= \frac{\lambda A^2}{2}\left[\sqrt{m^2-1}+\left(m^2-2\right)\arctan\sqrt{m^2-1}\right]+ \\ &\quad \frac{4\lambda^2 A}{3}\left(\sqrt{m^2-1}\arctan\sqrt{m^2-1}-m+1\right), \qquad (5) \\ \Delta &= A^2-\frac{4}{3}A\lambda\sqrt{m^2-1}\,, \text{ and} \qquad (6) \\ \bar{F}_{\mathrm{n}} &= A^3-\lambda A^2\left(\sqrt{m^2-1}+m^2\arctan\sqrt{m^2-1}\right). \qquad (7) \end{aligned}$$

This set of equations has been written in terms of the dimensionless values $A = a\sqrt[3]{\frac{K}{\pi\varpi R^2}}$, $\bar{F}_{\mathrm{n}} = \frac{F_{\mathrm{n}}}{\pi\varpi R}$, $\Delta = \delta\sqrt[3]{\frac{K^2}{\pi^2\varpi^2 R}}$ and $m = \frac{c}{a}$, with c the adhesive-contact radius on which adhesive forces apply, see Fig. 1(a). This last value is found to satisfy

$$\delta = \frac{a^2}{R}-\frac{8\sigma_0}{3K}\sqrt{c^2-a^2}\,, \qquad (8)$$

which completes the set of Eqns. (5-7). Note that this set of equations requires iterations to be solved, which makes the method difficult of use, *e.g.* for curve fitting. Simplified equations were derived by Carpick *et. al* [43], who provide a "rapid method of determining the value of the transition parameter".

Kim *et al.* [7] extended the Maugis-Dugdale solution to the non-contact regime, *i.e.* $a = 0$ and $c \neq 0$, see Fig. 1(b), by the adjustment of Maugis governing Eqns. (5-7), see [10] for details. Practically, this extennsion has to be considered when $\lambda < 0.938$.

As a general case, the determination of the contact force F_{n}, interference δ, and contact radius a can be found by solving Kim extension of/and Maugis theory for a given value of λ, which allows the dimensionless contact force $\bar{F}_{\mathrm{n}}$ to be expressed as a function of the dimensionless approach (interference) Δ. As this theory is purely elastic there is no difference between the loading and unloading conditions, as this model cannot account for pre-contact deformations [30] resulting from the adhesive effect. These deformations remain negligible apart for extremely compliant materials such as gold and are neglected herein. However, because of the elasto-plastic behavior happening during contact, the theory developed here below results in different adhesive-contact forces during loading $F_{\mathrm{n}}^{\mathrm{L}}(\delta)$ and unloading $F_{\mathrm{n}}^{\mathrm{U}}(\delta)$.

2.2.2. Adhesive Force on the Deformed Asperity

In literature models of the adhesive effects on plastically deformed asperities, the van der Waals forces are computed from the residual tip radius R_{res} obtained after plastic deformations [27], see Fig. 2. In the present work, in order to achieve better accuracy when compared to finite element simulations [31], we propose to account for a non-constant asperity radius in terms of the interference, see Fig. 2, and to perform the adhesive-contact theory on the assumed elastically deformed asperity who has an effective tip radius R_{eff} at a contact interference $\delta - \delta_{\mathrm{res}}$.

This assumption is motivated by the fact that Maugis theory assumes a uniform asperity radius to apply Hertz theory. However, during the interaction, this case is only met at the limit case $\delta = \delta_{\text{res}}$. If $\delta_{\text{res}} < \delta < \delta_{\max}$, the interaction occurs with a profile which is not spherical, and in order to account for this, we define an effective radius of the assumed elastically deformed asperity R_{eff}. Obviously when determining the profile, one should have $R_{\text{eff}}(\delta = \delta_{\text{res}}) = R_{\text{res}}$, where for a given loading process characterized by $\delta_{\max}$, the residual interference δ_{res} and the asperity tip radius R_{res} can be calculated from Eqns. (2-3). As the residual radius of curvature of the asperity profile is found to be larger at the summit than at other radial positions [27], $R_{\text{eff}}(\delta_{\text{res}} < \delta < \delta_{\max})$ should be lower than R_{res}, and a monotonic decreasing profile with δ is herein assumed, until reaching $R_{\text{eff}}(\delta_{\max}) = R\left[1 + c_1 1.275\left(\frac{S_Y}{E}\right)^{0.216}\left(\frac{\delta_{\max}}{\delta_{\text{CP}}} - 1\right)\right]$. Due to the isochoric behavior during plastic deformations, R_{eff} should be larger than R, and $c_1 < 1$ is a new parameter characterizing the effective curvature radius of the asperity at $\delta_{\max}$.

In this paper, we propose the expression

$$\frac{R_{\text{eff}}}{R} = \frac{R_{\text{res}}}{R} - 1.275\,(1 - c_1)\left(\frac{S_Y}{E}\right)^{0.216}\left(\frac{\delta_{\max}}{\delta_{\text{CP}}} - 1\right)\left(\frac{1 - e^{c_2\frac{\delta - \delta_{\text{res}}}{\delta_{\max} - \delta_{\text{res}}}}}{1 - e^{c_2}}\right), \tag{9}$$

where c_1 and c_2 are expressions determined by an inverse analysis in the following paragraphs.

2.2.3. Loading Process

During the loading process, when the interference δ is larger than the critical interference δ_{CP} (1), the current interference δ will be used as $\delta_{\max}$ the maximum interference reached. Thus $\delta_{\max} = \delta$ and both the residual interference δ_{res} and asperity tip radius R_{res} can be calculated from Eqns. (2-3). Therefore, the adhesive-contact force during loading $F_{\text{n}}^{\text{L}}(\delta)$ can be directly evaluated from the set of Eqns. (5-8) by substituting the asperity tip radius R by R_{eff} (9) and the interference δ by $\delta - \delta_{\text{res}}$. During the loading process δ_{res} keeps increasing.

2.2.4. Unloading Process

During the unloading procedure, the maximum interference $\delta_{\max}$ is a constant value determined at the end of the loading stage. Then, the residual interference δ_{res} is derived from $\delta_{\max}$ by Eqn. (2) and remains constant during the unloading procedure. Therefore, the adhesive-contact force during unloading $F_{\text{n}}^{\text{U}}(\delta)$ can be obtained from the adhesive theory by substituting the asperity tip radius R by R_{eff} (9) and the interference δ by $\delta - \delta_{\text{res}}$. However, contrarily to the loading process, the effect of adhesion needs to be considered at the intermediate pull-out stage, which is achieved by using the Kim *et al.* [7] extension of the Maugis-Dugdale adhesive-contact theory [6].

Table 1: Topology and material properties of Ru

R	E	ν	S_Y	z_0	ϖ
4 μm	410 GPa	0.3	3.42 GPa	0.169 nm	1 J/m^2

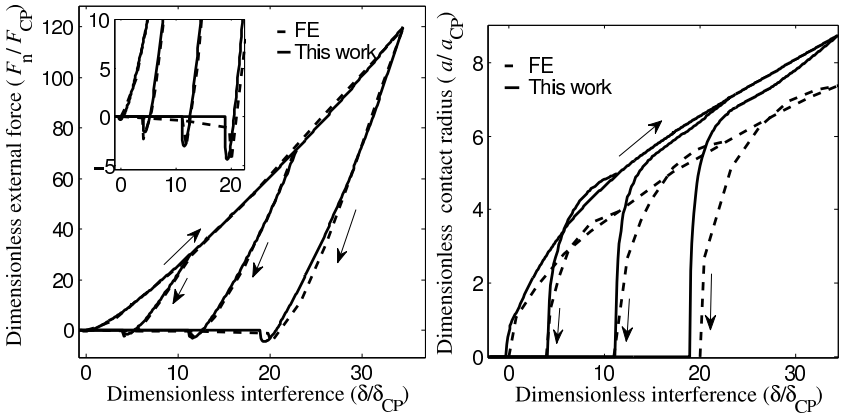

(a) Adhesive-contact force (b) Contact radius

Figure 3: Comparison between the model and FE results

2.2.5. Inverse Analysis

In order to identify the parameters c_1 and c_2 in the definition of R_{eff} (9), we use the finite element results carried out for the single asperity problem in [31]. In this work, the elasto-plastic adhesive contact of a micro sphere was studied for both Ruthenium (Ru) and Gold (Au) materials, which are classically used for electrical contacts. Because gold has an obvious adhesion induced plastic deformation during unloading, we only study the case of Ruthenium, which satisfies the elastic unloading assumption, see [32] for details. The surface and material properties considered in [31] are listed in Table 1. The adhesive energy was chosen "in consideration of the imperfect surface covered by impurity films when the testing is not done under the UHV conditions" [31].

From the analysis, we propose the expressions

$$c_1 = 0.22 + 0.6242e^{-0.092\frac{\delta_{\max}}{\delta_{\text{CP}}}}, \text{ and} \tag{10}$$

$$c_2 = \frac{10}{1+\left(\frac{\delta_{\max}}{10\delta_{\text{CP}}}\right)^2} - 5\,, \tag{11}$$

and show that the model predicts the correct behavior. Toward this end, we compare the loading and unloading adhesive-contact forces for three maximum interferences $\delta_{\max}$ successively equal to 17, 34 and 51 nm.

Results for loading and unloading are illustrated in Fig. 3(a) in terms of the dimensionless external force *vs.* the dimensionless interference, and in Fig. 3(b)

in terms of the dimensionless contact radius *vs.* the dimensionless interference. The maximum adhesive forces obtained are rather close to the finite element results, within 1%, which is better than actual models, see comparison achieved in [31]. Although the predicted contact radius has the same trend as the finite element results, the difference increases up to 15% with the increase of the maximum interference reached during the loading. This difference comes from the different assumptions made in our model and in the finite element simulation. This explains that similar results cannot be achieved for both the adhesive-contact force and for the contact radius from the same inputs as the relation between them is different. From the results comparisons, it is found that the coefficient c_1 has an obvious effect on the predicted adhesive-force, which is not sensitive to the coefficient c_2, which affects more the predicted contact radius.

The expressions of c_1 and c_2 are thus valid for the Ruthenium material. Although new expressions should perhaps be provided for other materials, the methodology should remain valid under the assumption of elastic unloading.

2.3. Parameters identification

In this section, many parameters are required to build the single asperity model. Some parameters are mechanical, as the Young modulus E, and the yield stress S_Y, and can be obtained from nano-indentation or micro tensile tests.

Beside these mechanical properties, the adhesive energy ϖ and the the critical separation distance z_0 have also to be determined. The adhesive energy per unit area ϖ is the energy required to separate two perfectly flat unit surfaces in contact. Based on a Lennard-Jones (LJ) potential, the expression of this adhesive energy is deduced from the work required to move the two half spaces from the equilibrium distance D_0 to infinity [6, 44], leading to

$$\varpi = \frac{A}{16\pi D_0^2}\,, \tag{12}$$

where A is the Hamaker constant. This Hamaker constant can be measured, in which case the effect of the surface contamination is taken into account, see [45, 46] for example. It can also be computed analytically, in which case the value is only valid in vacuum for perfectly clean surfaces. This analytic expression reads

$$A = 4\varepsilon\pi^2\rho_1\rho_2 r_0^6\,, \tag{13}$$

where ε is the potential energy between two atoms at equilibrium, where r_0 is the distance at which the inter-particle potential vanishes, and where ρ_1, ρ_2 are the volume densities of atoms of the two bodies. As demonstrated in [10, 44], when using the Maugis theory, the following relations between the distances hold

$$D_0 = \sqrt[6]{\frac{2}{15}}r_0 \quad \text{and} \quad z_0 = 0.97\sqrt[6]{2}r_0\,. \tag{14}$$

Finally the surface tension σ_0 follows from $\varpi = \sigma_0 z_0$.

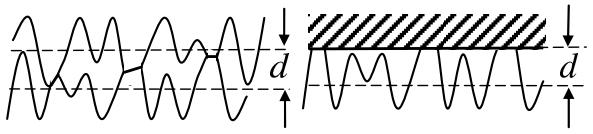

(a) Initial surfaces (b) Equivalent surface

Figure 4: Rough surfaces interaction at a separation distance d. (a) Contact of two rough surfaces. (b) Equivalent rough surface with smooth surface contact.

3. Rough Surfaces Interaction

In this section the micro adhesive-contact forces happening on a single asperity, as developed in the previous section, are integrated on statistical representations of the rough surfaces.

3.1. Characterization of the Rough Surfaces

According to the Greenwood and Williamson asperity-based model [8], an initial rough surface can be described by a collection of spherical asperities with identical end radius R, whose heights h have a Gaussian statistical distribution

$$\varphi(h) = \frac{1}{\sigma_s\sqrt{2\pi}} e^{-\frac{h^2}{2\sigma_s^2}}, \tag{15}$$

where σ_s is the standard deviation in the asperity height.

When two rough surfaces, of asperity tip end radii R_i and standard deviations in the asperity height σ_{si}, interact, as illustrated on Fig. 4(a), the problem can be substituted by the contact between an equivalent rough surface and a smooth plane with negligible difference [9, 47], see Fig. 4(b). Although this equivalence was first studied for elastic cases, it is also adopted for elasto-plastic cases [37]. The equivalent rough surface is thus characterized by the asperity tip radius

$$R = \frac{R_1 R_2}{R_1 + R_2}, \tag{16}$$

and by a standard deviation in the asperity height

$$\sigma_s = \sqrt{\sigma_{s1}^2 + \sigma_{s2}^2}. \tag{17}$$

Finally, the distance d, which is initially defined as the separation between the two mean planes of asperity height, Fig. 4(a), is now defined by the distance from the equivalent rough surface mean plane of asperity height to the smooth surface, Fig. 4(b).

3.2. Evaluation of the Micro Adhesive-Contact Forces

From section 2, the forces on each asperity $F_{\mathrm{n}}^{\mathrm{L}}(\delta)$, during loading, and $F_{\mathrm{n}}^{\mathrm{U}}(\delta)$, during unloading, are known in terms of the interference δ of this

asperity. Therefore, one can directly deduce the expression of the adhesive-contact forces per unit area $F_{\mathrm{nT}}^{\mathrm{L}}(d)$, during loading, and $F_{\mathrm{nT}}^{\mathrm{U}}(d)$, during unloading, in terms of the separation distance d. With the dimensionless quantities $\bar{F}_{\mathrm{nT}} = \frac{F_{\mathrm{nT}}}{\pi\varpi R}$, $\bar{d} = d\sqrt[3]{\frac{K^2}{\pi^2\varpi^2 R}}$, $\bar{\sigma}_s = \sigma_s\sqrt[3]{\frac{K^2}{\pi^2\varpi^2 R}}$, and dimensionless interference Δ, as $\delta = h - d$, these expressions read

$$\bar{F}_{\mathrm{nT}}^{\mathrm{L/U}}\left(\bar{d}\right) = \frac{N}{\bar{\sigma}_s\sqrt{2\pi}}\int_{\Delta_1^{\mathrm{L/U}}}^{\infty}\bar{F}_{\mathrm{n}}^{\mathrm{L/U}}(\Delta)\, e^{-\frac{(\Delta+\bar{d})^2}{2\bar{\sigma}_s^2}}\mathrm{d}\Delta\,, \tag{18}$$

for respectively loading and unloading processes. In these last two expressions, $\Delta_1^{\mathrm{L}} = 0$ and $\Delta_1^{\mathrm{U}} < 0$ are respectively the loading and unloading dimensionless integration limits for which adhesive forces are active. During the unloading process, $\Delta_1^{\mathrm{U}} = -\frac{2}{\pi\lambda}$ when Kim extension is considered, *i.e.* for $\lambda < 0.938$. In the other case, there is an abrupt pull-out, see [10] for details.

In order to compute Eqn. (18), the expressions of the forces on each asperity $\bar{F}_{\mathrm{n}}^{\mathrm{L/U}}(\Delta)$, for respectively the loading/unloading processes, are computed following Section (2.2). However, asperities enter in plasticity for different interferences, due to the statistical height distribution, and the effective profile is different for each asperity. A change of variable leads to

$$\bar{F}_{\mathrm{n}}^{\mathrm{L/U}}(\Delta) = \bar{F}_{\mathrm{n}}^{\mathrm{L/U}}(\Delta',\,\lambda')\,\frac{\pi\varpi R_{\mathrm{eff}}}{\pi\varpi R}\,, \tag{19}$$

where $\Delta' = (\delta - \delta_{\mathrm{res}})\sqrt[3]{\frac{K^2}{\pi^2\varpi^2 R_{\mathrm{eff}}}}$, $\Delta = \delta\sqrt[3]{\frac{K^2}{\pi^2\varpi^2 R}}$, and $\lambda' = 2\sigma_0\sqrt[3]{\frac{R_{\mathrm{eff}}}{\pi\varpi K^2}}$. Thus, during the integration (18), for updated values Δ' and λ', $\bar{F}_{\mathrm{n}}^{\mathrm{L/U}}(\Delta',\,\lambda')$ is computed using explicitly the framework defined in Section (2.2).

3.3. Evaluation of the cyclic loading effect

The cyclic loading effect can be studied by repeating the loading/unloading analyzes with updated asperities profiles. Indeed, after one cycle the profile of the surface is modified as only higher asperities enter into contact and exhibit plastic deformations. History is tracked by keeping after each loading the function $\delta_{\max}(h)$ of the maximal interference reached for one asperity of initial height h. Thus, the profile change of an asperity of initial height h is known and can be used to evaluate its effect on the loading/unloading forces (18).

3.4. Parameters identification

One surface is characterized by the asperity tip end radius R, the standard deviation in asperity height σ_s, but also by the number of asperities per surface area N. These values can be identified from the study of the surface topography, and, in particular, depend on the surface RMS roughness R_q. Practically, the statistical surface parameters of the GW model can be calculated following the method proposed by McCool [48], see also [12] for details, which is briefly summarized here below.

Table 2: Parameters for the 1D application

d_0	t_d	ε_0	$\frac{\varepsilon_\mathrm{d}}{\varepsilon_0}$	t_s
1-3 μm	0.15 μm	8.854 pF/m	7.6	180 nm

The variance of the height m_0, the variance of the slope m_2, and the variance of the curvature m_4 can be evaluated from the surface topography $z\,(x,\,y)$ [49],

$$m_0 = \left\langle z^2 \right\rangle \,, \quad m_2 = \left\langle \frac{dz}{dx} \right\rangle \,, \quad \text{and } m_3 = \left\langle \frac{d^2z}{dx^2} \right\rangle \,, \tag{20}$$

where x is an arbitrary direction, and where $\langle\rangle$ represents a statistical average. Remark that one has directly $R_q = \sqrt{m_0}$ by definition of the RMS roughness. Following the work of McCool [48], the surface is characterized by

$$R = \frac{3}{8}\sqrt{\frac{\pi}{m_4}}\,, \tag{21}$$

$$N = \frac{m_4}{6\pi\sqrt{3}m_2}\,, \text{ and} \tag{22}$$

$$\sigma_s = \sqrt{m_0 - \frac{3.717 \times 10^{-4}}{N^2R^2}}\,. \tag{23}$$

The surface topography $z\,(x,\,y)$ can be obtained from AFM measurements. As the apparatus resolutions and sample lengths affect these surface parameters, which, in turn, will affect the application of the rough surface contact theory [50], a sample of length L, which is comparable to the characteristic dimension of the MEMS structure, is suggested during the measurements of the statistical characteristics of the surface.

For the interaction of two rough surfaces, R_i and σ_{si} of the two surfaces can be obtained from respectively Eqns. (21) and (23). The equivalent radius R and the equivalent standard deviation in asperity height σ_s are then deduced directly from respectively Eqns. (16) and (17). This same relation also holds for the equivalent RMS roughness, *i.e.* $R_q = \sqrt{R_{q1}^2 + R_{q2}^2}$, and an equivalent m_0 is thus deduced directly. From this last value and from the equivalent asperity tip end radius R and the equivalent standard deviation in asperity height σ_s, the equivalent asperities surface density N can be computed from Eqn. (23).

4. Application to a 1D Micro-Switch

In this section we apply the previously developed model to study a micro-switch. To study a complex structure, the micro adhesive-contact model should be coupled with a finite element code, so as a way of illustration we consider the equivalent 1D model illustrated in Fig. 5(a).

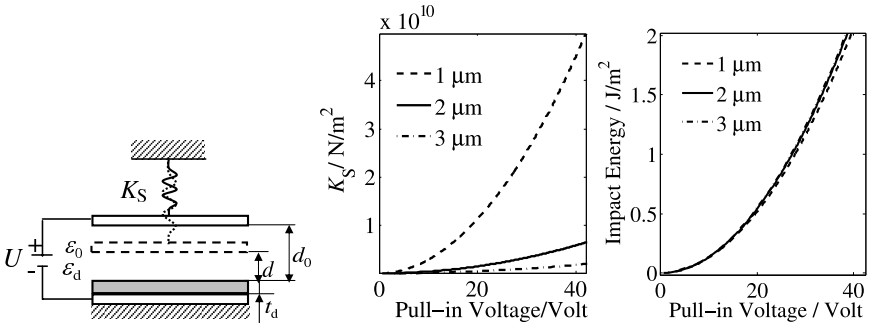

(a) Schematics (b) Stiffness (c) Impact energy

Figure 5: 1D micro-switch. (a) Model. (b) Stiffness K_{S} in terms of pull-in voltage $U_{\text{pull-in}}$ for different initial gaps d_0. (c) Impact energy E_{I} in terms of pull-in voltage $U_{\text{pull-in}}$ for different initial gaps d_0

Table 3: Ru-Ru contact topography

Sample	R_q	σ_s	R	N
A	2.03 nm	1.97 nm	4 μ m	10 $\mu\mathrm{m}^{-2}$
B	3.99 nm	3.96 nm	4 μ m	10 $\mu\mathrm{m}^{-2}$
C	7.81 nm	7.78 nm	4 μ m	10 $\mu\mathrm{m}^{-2}$

In this model, a movable electrode is attached to a spring, and a potential difference U is applied between it and a substrate electrode covered by a dielectric layer. The switch is supposed to work in vacuum, so the damping effect of the squeeze film is neglected. This model is characterized by K_{S} the stiffness of the equivalent restoring spring per unit area of the movable electrode, d_0 the initial gap between the movable electrode and the dielectric layer, t_{d} the thickness of this dielectric layer, and by ε_0 and ε_{d} the permittivity of vacuum and of the dielectric layer respectively. Typical values for SiN dielectrics are reported in Table 2.

The contact is assumed to occur between two Ru surfaces, for which typical topography values are reported in Table 3. The three statistical surface parameters of the GW model can be calculated following the method detailed in the previous section. The roughness of a Ru film under different deposit methods was measured by Kim *et al.* [51], the initial tip radius R is the one studied in Section 2.2, and the asperity density N is a typical value for deposition. Ru films are deposited on the movable electrode, and also on a part of the substrate, and are characterized by a thickness t_{s} and a Young modulus E_{s}. Typical value for the Ru film thickness is reported in Table 2 [52], and the Young modulus is the one reported in Table 1.

4.1. Impact Energy

It can be shown that during the pull-in study, the distance between the movable electrode and the substrate layer can be assimilated to the separation d between the two mean planes of the rough surfaces [10]. Thus, neglecting fringing of the electrical field, the electrostatic force before contact between the electrodes and the restoring force of the spring respectively read

$$F_{\mathrm{E}} = -\frac{\varepsilon_0 U^2}{2\left(d + \frac{\varepsilon_0 t_{\mathrm{d}}}{\varepsilon_{\mathrm{d}}}\right)^2}, \text{ and } F_{\mathrm{S}} = K_{\mathrm{S}}\left(d_0 - d\right). \tag{24}$$

These two forces are both per surface area of the movable electrode.

Once the DC Voltage U reaches the pull-in voltage $U_{\text{pull-in}}$ of the device, the movable electrode crashes on the substrate electrode. The pull-in voltage and the distance at pull-in $d_{\text{pull-in}}$ can be evaluated as [53]

$$U_{\text{pull-in}} = \sqrt{\frac{8K_{\mathrm{S}}}{27\varepsilon_0}\left(d_0 + \frac{\varepsilon_0 t_{\mathrm{d}}}{\varepsilon_{\mathrm{d}}}\right)^3}, \text{ and} \tag{25}$$

$$d_{\text{pull-in}} = \frac{2d_0 - \frac{\varepsilon_0 t_{\mathrm{d}}}{\varepsilon_{\mathrm{d}}}}{3}. \tag{26}$$

The Fig. 5(b) plots the pull-in voltage $U_{\text{pull-in}}$ for different designs characterized by different values of the spring stiffness K_{S} and of the initial gap d_0.

In order to assess the stiction risk, the impact energy per unit area of the movable electrode, E_{I}, is determined as it influences the plastic deformation of the asperities and thus the adhesive-contact forces. From Eqn. (24), the impact energy per unit area E_{I} can readily be evaluated as

$$E_{\mathrm{I}} = \int_0^{d_{\text{pull-in}}} \left[\frac{\varepsilon_0 U_{\text{pull-in}}^2}{2\left(d + \frac{\varepsilon_0 t_{\mathrm{d}}}{\varepsilon_{\mathrm{d}}}\right)^2} - K_{\mathrm{S}}\left(d_0 - d\right)\right] \mathrm{d}d\,. \tag{27}$$

In this equation, the lower integral bound 0 is a reasonable approximation stating that compared to the displacement before contact, the movable electrode has a trivial displacement from entering contact till its velocity reaches zero.

For values reported in Table 2, the impact energy (27) is reported in Fig. 5(c) for different pull-in voltages (25) and initial gaps d_0. Although the real electrostatic force actuated switches have a more complex structure than the one on Fig. 5(a), this 1D model can give us a general idea of the dimension of impact energy. From Fig. 5(c), it can be found that the impact energy has an obvious relation to the designed pull-in voltage.

4.2. Loading Phase

After pull-in, the electrode impacts the Ru film contact pad. Although practically the surface of the contacting surface is not equal to the surface of the movable electrode, Fig. 5(c) is used to illustrate our discussion by choosing

impact energies $E_{\mathrm{I}} = 0.5$, 1.0 and 2.0 J/m^2. However this energy is per surface area of the contacting Ru contact pad.

Once the impact occurs, the energy E_{I} is converted into a strain energy stored in the deformed asperities and an elastic wave propagation. The strain energy might include not only the elastic strain energy, but also the plastic strain energy when the impact energy is high enough. This loading process will finish once all the energy has been converted.

Two interacting surfaces do not remain glued at the first time they contact. The movable electrode bounces several times before making permanent contact with the substrate [54]. For simplification, all plastic deformations of asperities can be assumed to occur during the first contact, and subsequent loading and unloading processes are assumed to remain purely elastic [55]. Since the impact energy will be dissipated by the plastic deformation of the material and by the other damping effects during the bouncing sub-cycles, this simplification assumption is reasonable. The energy for the elastic wave propagation is neglected in this work, however elastic energy in the Ru film is accounted for.

With these assumptions, the distance d_e, between the two rough surfaces mean planes of asperity height, reached at the end of the impact process is deduced from

$$E_{\mathrm{I}} = \int_{d_e}^{\infty} F_{\mathrm{nT}}^{\mathrm{L}}(d)\,\mathrm{d}d + \frac{\left[F_{\mathrm{nT}}^{\mathrm{L}}(d_e)\right]^2 t_{\mathrm{s}}}{2E_{\mathrm{s}}}\,, \tag{28}$$

where the loading adhesive-contact force $F_{\mathrm{nT}}^{\mathrm{L}}$ results from Eqn. (18). The second term of Eqn. (28) results from the elastic energy in the Ru film.

4.3. Unloading Phase

Once the minimal distance d_e has been computed from Eqn. (28), the unloading adhesive-contact force $F_{\mathrm{nT}}^{\mathrm{U}}$ is obtained from Eqn. (18). This normalized adhesive contact force *vs.* the normalized distance is presented in Figs. 6(a)-6(c), for the three different surface samples, A-C respectively, reported in Table (3) and for the three different impact energies E_{I}. Note that the curves show the parts for $d > d_e$, which corresponds to unloading, but also the parts $d < d_e$, which corresponds to further loading and not unloading.

For the three surfaces, the adhesive force increases with the increase of the impact energy. For a given distance d, the elasto-plastic adhesive-contact forces are lower than the results obtained with the elastic theory [10]. From Fig. 6 we can find that, for E_{I}=0.5 J/m^2, the pull-out force with the plastic effect is 10 times higher compared to the curve obtained with the elastic theory. This ratio reaches more than 20 for E_{I}=2 J/m^2.

This difference becomes more obvious for surfaces with a higher roughness (sample C). Indeed when the roughness increases, the higher asperities are more subject to plastic deformations as only a reduced number of them enter into contact, increasing the adhesive force. For a low roughness, more asperities enter into contact at the same time, thus reducing the plastic deformations, and most of the asperities deform elastically.

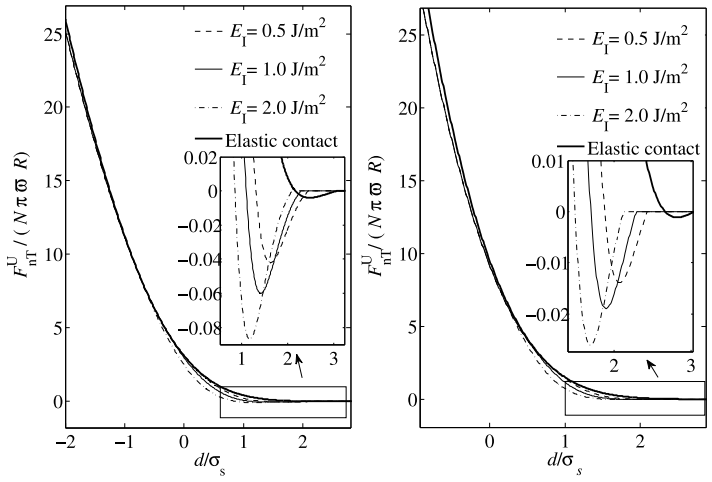

(a) Sample A

(b) Sample B

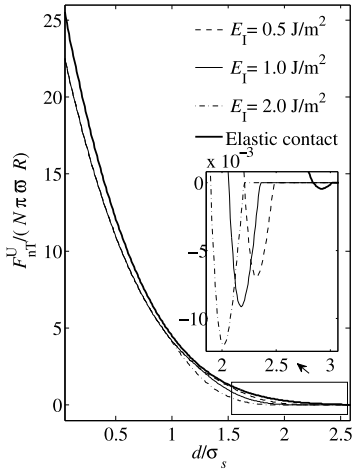

(c) Sample C

Figure 6: Unloading curves for different impact energies and different surface properties

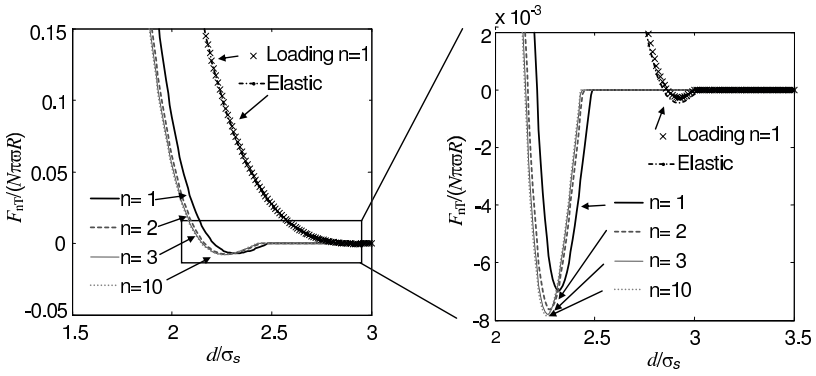

Figure 7: Effect of cyclic loading

4.4. Cyclic loadings

The cyclic loading effect is studied following the analysis described in section 3.3 for the C sample, see Table 3, and for an impact energy E_{I}=0.5 J/m^2 [56]. The reliability of the micro-switch is studied by considering the effect of repeated interactions between the movable/substrate electrodes. As it can be seen on Fig. 7, where results after one, two, three and ten cycles are reported, the unloading curves change after each interaction until reaching accommodation. From this figure it appears that the pull-out force after accommodation can be predicted, opening the way to a stiction-free design. The elastic solution is also reported on Fig. 7, and is shown to underestimate the pull-out force.

5. Conclusions

In this paper we present an analytical model predicting the adhesive-contact forces during the interaction of two rough elasto-plastic surfaces of MEMS devices working in dry environment. The model is limited to metals exhibiting a reduced amount of plasticity during the contact. Although parameters have been identified from finite element simulations for Ruthenium, the methodology should remain valid for other materials, under the assumption of elastic unloading.

The predictions of this model are illustrated using a simpler 1D switch application. It is shown that the impact energy at the contact point has an important effect on the adhesive force between the contacted rough surfaces, as the plastic deformations depend on this energy.

Finally, it is shown that the cyclic usage of the MEMS switch changes the structure of the contacting surfaces due to the plastic deformations. With time, the contact surfaces become smoother, increasing the adhesive effect, and stiction might happen after the device has been used for a period of time. This effect should be considered at the design stage to avoid in-use stiction.

In the near future it is intended to couple the developed micro-model with structural finite element analyzes, for which contacts are modeled using the

adhesive-contact forces predicted in this paper. Such a multi-scale analysis has been developed by the authors in the elastic case and will be extended to this elasto-plastic framework by considering dynamic simulations. In that case the impact energy will be known from the finite element simulation via the nodal velocities, and the developed approach can be readily applied.

References

[1] W. van Spengen, MEMS reliability from a failure mechanisms perspective, Microelectronics Reliability 43 (7) (2003) 1049–1060.

[2] W. van Spengen, R. Puers, I. De Wolf, On the physics of stiction and its impact on the reliability of microstructures, Journal of Adhesion Science and Technology 17 (4) (2003) 563–582(20).

[3] G. G. Adams, N. E. McGruer, A Review of Adhesion in an Ohmic Microswitch, Journal of Adhesion Science and Technology 24 (15-16) (2010) 2571–2595, doi:10.1163/016942410X508154, URL http://www.tandfonline.com/doi/abs/10.1163/016942410X508154.

[4] K. Johnson, K. Kendall, A. Roberts, Surface energy and the contact of elastic solids, Proceedings of the Royal Society ofLondon A 324 (1558) (1971) 301–313.

[5] B. Derjaguin, V. Muller, Y. Toporov, Effect of contact deformation on the adhesion of elastic solids, Journal of Colloid and Interface Science 53 (2) (1975) 314–326.

[6] D. Maugis, Adhesion of spheres: The JKR–DMT transition using a Dugdale model, Journal of Colloid and Interface Science 150 (1) (1992) 243–269.

[7] K. Kim, R. McMeeking, K. Johnson, Adhesion, slip, cohesive zones and energy fluxes for elastic spheres in contact, Journal of the Mechanics and Physics of Solids 46 (2) (1998) 243–266.

[8] J. Greenwood, J. Williamson, Contact of nominally flat surfaces, Proceedings of the Royal Society ofLondon A 295 (1442) (1966) 300–319.

[9] J. Greenwood, J. Tripp, The contact of two nominally flat rough surfaces, Proceedings of the Institution of Mechanical Engineers 1847-1996 185 (1970) (1971) 625–633.

[10] L. Wu, V. Rochus, L. Noels, J.-C. Golinval, Influence of adhesive rough surface contact on microswitches, Journal of Applied Physics 106 (11) (2009) 113502–1 – 113502–10.

[11] C. Do, M. Hill, M. Lishchynska, M. Cychowski, K. Delaney, Modeling, simulation and validation of the dynamic performance of a single-pole single-throw RF-MEMS contact switch, in: Thermal, Mechanical & Multi-Physics

Simulation, and Experiments in Microelectronics and Microsystems (EuroSimE), 2011 12th International Conference on, 1–6, linz, Austria, 2011.

[12] L. Wu, L. Noels, V. Rochus, M. Pustan, J.-C. Golinval, A micro-macroapproach to predict stiction due to surface contact in microelectromechanical systems, Journal of Microelectromechanical Systems 20 (4) (2011) 976–990.

[13] N. Tas, T. Sonnenberg, R. Legtenberg, E. M., Stiction in surface micromachining, Journal of Micromechanics and Microengineering 6 (4) (1996) 385–397.

[14] M. de Boer, J. Knapp, M. Mayer, T. Michalske, Role of interfacial properties on MEMS performance and reliability, in: Microsystems Metrology and Inspection, vol. **3825**, SPIE, 2–15, munich, Germany, 1999.

[15] R. Jones, Models for contact loading and unloading of a rough surface, International Journal of Engineering Science 42 (17-18) (2004) 1931 – 1947.

[16] J. Williams, The influence of repeated loading, residual stresses and shakedown on the behaviour of tribological contacts, Tribology International 38 (9) (2005) 786 – 797, special Issue in Memory of Professor Tony Ball.

[17] S. Majumder, N. McGruer, G. Adams, P. Zavracky, R. Morrison, J. Krim, Study of contacts in an electrostatically actuated microswitch, Sensors and Actuators A: Physical 93 (1) (2001) 19 – 26.

[18] F. F. Abbott E., Specifying surface qualitya method based on accurate measurement and comparison, Mechanical Engineering 55 (2) (1933) 569 – 572.

[19] R. Jackson, I. Green, A Finite Element Study of Elasto-Plastic Hemispherical Contact Against a Rigid Flat, Journal of Tribology 127 (2) (2005) 343 – 354.

[20] W. Chang, I. Etsion, D. Bogy, An elasticplastic model for the contact of rough surfaces, Journal of Tribology 109 (2) (1987) 257–263.

[21] P. Sahoo, A. Banerjee, Asperity interaction in adhesive contact of metallic rough surfaces, Journal of Physics D: Applied Physics 38 (22) (2005) 4096–4103.

[22] Y. Peng, Y. Guo, An adhesion model for elastic-plastic fractal surfaces, Journal of Applied Physics 102 (5) (2007) 053510–1–053510–7.

[23] L.-Y. Li, C.-Y. Wu, C. Thornston, A theoretical model for the contact of elastoplastic bodies, Proceedings of the Institution of Mechanical Engineers, Part C: Journal of Mechanical Engineering Science 216 (4) (2001) 421 – 431.

[24] L. Kogut, I. Etsion, Elasticplastic contact analysis of a sphere and a rigid flat, Journal of Applied Mechanics 69 (5) (2002) 657–662.

[25] L. Kogut, I. Etsion, Adhesion in elastic-plastic spherical microcontact, Journal of Colloid and Interface Science 261 (2) (2003) 372 – 378.

[26] V. Brizmer, Y. Kligerman, I. Etsion, The effect of contact conditions and material properties on the elasticity terminus of a spherical contact, International Journal of Solids and Structures 43 (18-19) (2006) 5736 – 5749.

[27] I. Etsion, Y. Kligerman, Y. Kadin, Unloading of an elastic-plastic loaded spherical contact, International Journal of Solids and Structures 42 (13) (2005) 3716 – 3729.

[28] S. Mohamed Ali, P. Sahoo, Adhesive friction for elasticplastic contacting rough surfaces using a scale-dependent model, Journal of Physics D: Applied Physics 39 (4) (2006) 721–729.

[29] X. Xue, A. A. Polycarpou, Meniscus model for noncontacting and contacting sphere-on-flat surfaces including elastic-plastic deformation, Journal of Applied Physics 103 (2) 023502, doi:10.1063/1.2830863.

[30] P. Attard, J. Parker, Deformation and adhesion of elastic bodies in contact, Physical Review A 46 (12) (1992) 7959–7971.

[31] Y. Du, L. Chen, N. McGruer, G. Adams, I. Etsion, A finite element model of loading and unloading of an asperity contact with adhesion and plasticity, Journal of Colloid and Interface Science 312 (2) (2007) 522 – 528.

[32] Y. Kadin, Y. Kligerman, I. Etsion, Jump-in induced plastic yield onset of approaching microcontacts in the presence of adhesion, Journal of Applied Physics 103 (1) (2007) 013513–1–013513–8.

[33] Y. Kadin, Y. Kligerman, I. Etsion, Cyclic loading of an elasticplastic adhesive spherical microcontact, Journal of Applied Physics 104 (7) (2007) 073522–1–073522–8.

[34] L. Pei, S. Hyun, J.-F. Molinari, M. Robbins, Finite element modeling of elasto-plastic contact between rough surfaces, Journal of the Mechanics and Physics of Solids 53 (11) (2005) 2385 – 2409.

[35] R. Ardito, A. Corigliano, A. Frangi, Finite Element modelling of adhesion phenomena in MEMS, in: Thermal, Mechanical & Multi-Physics Simulation, and Experiments in Microelectronics and Microsystems (EuroSimE), 2010 11th International Conference on, 1–6, bordeau, France, 2010.

[36] R. L. Jackson, I. Green, A statistical model of elasto-plastic asperity contact between rough surfaces, Tribology International 39 (9) (2006) 906 – 914, ISSN 0301-679X, doi:10.1016/j.triboint.2005.09.001.

[37] Y. Kadin, Y. Kligerman, I. Etsion, Unloading an elastic-plastic contact of rough surfaces, Journal of the Mechanics and Physics of Solids 54 (12) (2006) 2652 – 2674.

[38] R. Jackson, S. J.L., A multi-scale model for contact between rough surfaces, Wear 261 (11 - 12) (2006) 1337 – 1347, ISSN 0043-1648, doi: 10.1016/j.wear.2006.03.015.

[39] L. Almeida, R. Ramadoss, R. Jackson, K. Ishikawa, Q. Tu, Laterally actuated multicontact MEMS relay fabricated using MetalMUMPS process: experimental characterization and multiscale contact modeling, Journal of Micro/Nanolithography, MEMS and MOEMS 6 (2) 023009, doi: 10.1117/1.2744240.

[40] R. L. Jackson, I. Green, On the Modeling of Elastic Contact between Rough Surfaces, Tribology Transactions 54 (2) (2011) 300–314, doi: 10.1080/10402004.2010.542277.

[41] S. Mukherjee, S. M. Ali, P. Sahoo, An improved elastic-plastic contact model of rough surfaces in the presence of adhesion, Proceedings of the Institution of Mechanical Engineers, Part J: Journal of Engineering Tribology 218 (6) (2004) 557–568, doi:10.1243/1350650042794789.

[42] K. Komvopoulos, W. Yan, Three-Dimensional Elastic-Plastic Fractal Analysis of Surface Adhesion in Microelectromechanical Systems, Journal of Tribology 120 (4) (1998) 808–813, doi:10.1115/1.2833783.

[43] R. W. Carpick, D. F. Ogletree, M. Salmeron, A General Equation for Fitting Contact Area and Friction vs Load Measurements, Journal of Colloid and Interface Science 211 (2) (1999) 395 – 400, ISSN 0021-9797, doi: 10.1006/jcis.1998.6027.

[44] N. Yu, A. A. Polycarpou, Adhesive contact based on the LennardJones potential: a correction to the value of the equilibrium distance as used in the potential, Journal of Colloid and Interface Science 278 (2) (2004) 428 – 435, ISSN 0021-9797, doi:10.1016/j.jcis.2004.06.029, URL http://www.sciencedirect.com/science/article/pii/S0021979704005454.

[45] A. Plößl, G. Kräuter, Wafer direct bonding: tailoring adhesion between brittle materials, Materials Science and Engineering: R: Reports 25 (1-2) (1999) 1 – 88, ISSN 0927-796X, doi:10.1016/S0927-796X(98)00017-5.

[46] B. Cappella, G. Dietler, Force-distance curves by atomic force microscopy, Surface Science Reports 34 (1-3) (1999) 1 – 104, ISSN 0167-5729, doi: 10.1016/S0167-5729(99)00003-5.

[47] M. O'Callaghan, M. Cameron, Static contact under load between nominally flat surfaces in which deformation is purely elastic, Wear 36 (1) (1976) 79 – 97.

[48] J. McCool, Predicting Microfracture in Ceramics Via a Microcontact Model, Journal of Tribology 108 (1986) 380 – 386, ISSN 0043-1648, doi: 10.1016/j.wear.2006.03.015.

[49] R. Carpick, E. Flater, J. VanLangendon, M. de Boer, Friction in MEMS: From single to multiple asperity contact, in: Conference Proceedings of SEM VIII International Congress and Exposition on Experimental and Applied Mechanics, 282–287, 2002.

[50] L. Kogut, R. Jackson, A Comparison of Contact Modeling Utilizing Statistical and Fractal Approaches, Journal of Tribology 128 (1) (2006) 213–217, doi:10.1115/1.2114949.

[51] J. Kim, M. Kim, D. Yoon, Effects of an Added Iodine Source (C2H5I) on Ru MetalOrganic Chemical Vapor Deposition, Chemical Vapor Deposition 9 (2) (2003) 105–109.

[52] M. Walker, C. Nordquist, D. Czaplewski, G. Patrizi, N. McGruer, J. Krim, Impact of in situ oxygen plasma cleaning on the resistance of Ru and Au-Ru based rf microelectromechanical system contacts in vacuum, Journal of Applied Physics 107 (8) (2010) 084509–1 – 084509–7.

[53] M. Zahn, Electromagnetic Field Theory: A Problem Solving Approach, John Wiley & Sons, New-York, 1979.

[54] B. McCarthy, G. Adams, N. McGruer, D. Potter, A Dynamic Model, Including Contact Bounce, of an Electrostatically Actuated Microswitch, Journal of Microelectromechanical Systems 11 (3) (2002) 276–283.

[55] Z. Guo, N. McGruer, G. Adams, Modeling, simulation and measurement of the dynamic performance of an ohmic contact, electrostatically actuated RF-MEMS switch, Journal of Micromechanics and Microengineering 17 (9) (2007) 1899–1909.

[56] L. Wu, J.-C. Golinval, L. Noels, Stiction failure in microswitches due to elasto-plastic adhesive contacts, in: Conference Proceedings of the Society for Experimental Mechanics Series 42, vol. 6, 9, doi:10.1007/978-1-4614-4436-7_11, 2013.